Numerical and analytical investigation of the possibilities to enhance the thermal conductivity of core-shell particle packed beds

Deridder, Sander; Smits, Wim; Benkahla, Hamza; Broeckhoven, Ken; Desmet, Gert

Published in:
Journal of Chromatography A

DOI:
10.1016/j.chroma.2018.08.056

Publication date:
2018

- Detailed calculations of the effective heat conductivity in packed beds were made
- Silica cores contribute less than previously assumed to the effective conductivity
- Even high conductivity cores can only be expected to have a minimal effect
- A physically more sound alternative for the Zarichnyak-model is proposed
- Two conceptual other strategies to enhance the effective conductivity are discussed

Numerical and Analytical Investigation of the Possibilities to Enhance the Thermal Conductivity of Core-shell Particle Packed Beds

Sander Deridder [1], Wim Smits [1], Hamza Benkahla [1], Ken Broeckhoven [1], Gert Desmet [1,*]

[1] Vrije Universiteit Brussel, Pleinlaan 2, 1050 Brussel, Belgium
[*] Corresponding author: email: gedesmet@vub.be
tel.: ++3226293251
fax.: ++3226293248

Declarations of interest: none

Abstract

We report on a numerical study of the thermal conductivity of core-shell particle packed bed columns. Covering a variety of packing structures and a broad range of mobile phase and porous zone conductivities, it was in all cases found that switching to particles with a highly conducting core (e.g., with a gold or copper core instead of a silica core) would produce a much smaller increase of the effective heat conductivity of the bed (k_{eff}) than previously expected in literature. We found maximal increases on the order of some 20-70%, which is much lower than the potential increases up to 2000% assumed in literature. The overestimation in literature could be attributed to the fact that this literature was based on an incorrect extrapolation of the Zarichnyak-model which was the heat conductivity model predominantly used up till now. On the other hand, the computed relationships between k_{eff} and the core conductivity obtained in the present study are in good agreement with an analytical solution derived from the effective medium theory, a theory which is physically much more relevant for the case at hand than the Zarichnyak-model. The results also show that the observed increase in effective bed conductivity between fully porous and core-shell particle beds frequently observed in literature is not only due to the presence of the core, but that differences in the shell layer conductivity can play an equally important role. In addition, it could also be demonstrated that, if ways could be found to increase the conductivity of the shell layer, this would produce a much stronger increase of the overall bed conductivity than will ever be possible by increasing the conductivity of the cores.

Keywords: Thermal conductivity; Computational Fluid Dynamics; Core-shell particles; Effective Medium Theory

1. Introduction

Ever since the emergence of liquid chromatography, an evolution towards the use of smaller sized particles exists. Nowadays, (U)HPLC columns packed with sub 2 µm particles are being used in routine separations. These smaller particles induce higher backpressures, which lead to increased frictional heating. In this evolution, frictional heating poses an important problem, as it is one of the reasons preventing a further increase of the operating pressures that can be used in UHPLC. For example, for an operating pressure of 2500 bar, a temperature increase up to 54°C (water) or 85°C (methanol) is expected for a perfectly insulated column. Although this will in practice be lower due to heat losses from the column to the surrounding air in the thermostatted column compartment, temperature increases up to 56°C on a 10 cm long column (2.1 mm ID) have recently been measured when using methanol as a mobile phase at an operating pressure of 2600 bar [1]. For such large temperature increases, it is clear that near the end of the column, retention, and thus separation, will disappear [2]. Any attempt to remove the heat from the column will however cause a radial variation of the temperature in the particle bed, which in turn causes a radial variation of both viscosity and retention factor. As a result, the main velocity profile will no longer be plug flow-like but will be warped and parabolic-like, causing a very strong extra band broadening which can even lead to peak splitting [3].

Although coupled columns with intermediate cooling provide a potential solution [4], there is still a lot of interest in developing solutions for a more efficient heat removal in single column systems. One frequently cited solution is based on the concept of core-shell particles. Whereas the core does not contribute anything to the separation, it has been suggested to use this zone to increase the overall heat conductivity of the bed by replacing the conventional silica core by a core of a material with a much higher conductivity. Whereas silica typically has a heat conductivity of 1.38 W/(m·K) [5], materials such as gold and copper have a much higher conductivity (resp. 315 and 398 W/(m·K)) at room temperature [6].

As expressed by Fourrier's heat transfer law, the thermal conductivity (k) of a medium relates the flux of heat ($\vec{q}$ [W/m²]) to the spatial gradient of the temperature (∇T):

$$\vec{q} = k\nabla T \tag{1}$$

The relevant gradient for the removal of frictional heat in a chromatographic column is the radial gradient, because this is the one leading to the formation of a radial trans-column velocity gradient [7], in turn leading to an additional contribution to band broadening [8-10].

Although a few studies exist where attempts were made to assess the importance of radial heat transfer in contemporary UHPLC columns [9,11,12], the present study aims at investigating the problem at the microscopic level, using numerical methods and establishing analytical expressions for the effective heat conductivity of the bed based on the detailed geometry of the particles and the packing.

As a physical validation of our numerical results, they have been compared with the effective conductivity predicted by the effective medium theory [13,14]. This theory has already proven to be of great use to predict the effective diffusion in packed bed media [15-19].

2. Numerical methods

2.1. Geometry

Fig. 1 gives an overview of all considered packed bed geometries. The three first ones (Figs. 1a-c) represent three possible ordered sphere packings: the face centered cubic packing (fcc), the body centered cubic packing (bcc) and the simple cubic packing (sc). By mirroring the cubic cell in the figure over its six outer surfaces, an infinitely wide fcc, bcc or sc sphere packing is obtained. In each of the three cases, the geometries were attributed an external porosity (ε_e) of 0.40. An extra unit cell representing an fcc packing with porosity 0.24 (resulting in contacting particles, see detailed description further on) was considered as well (Fig. 1d). To investigate one of the hypotheses made in Section 3.3, a variant of the sc packing (also with ε_e=0.40) was constructed by connecting the core of each particle with the cores of its six closest neighboring particles using a cylindrical connection bridge (radius r_b=1.61x10^{-7} m) having the same properties as the core (Fig. 1e). A version with a smaller cylinder radius (r_b=1.15x10^{-7} m) was used as well.

Besides these ordered packings, a random packing was considered as well (Fig. 1f). For this purpose a random packing, already used in earlier work on mass diffusion [18], was reused in this study. The packing was generated with a numerical packing simulator (Macropac, Intelligensys) using a dynamic drop and roll algorithm to fill a container of square section with spheres of constant diameter. Because the first and last particle layers pack differently, these layers were discarded by only considering the middle section of the container, resulting in a cube packed with 73 spheres and an external porosity of 0.39. To avoid wall effects on the 4 sidewalls (besides the top and bottom), periodic sidewalls were used during packing.

To avoid numerical problems with singular contact points in the closest fcc packing case in Fig. 1d, the distance between neighboring particles was shrunk by 1%, thus creating a slight overlap and resulting in an actual external porosity of 0.24 and a contacting area between the spheres of 3% of the cross sectional area of an individual particle. It should be remarked that in a real column particles probably also make contact over a finite area rather than only in a singular point. The actual value of the contact surface is to the best of our knowledge not known. Extra information on this procedure can be found in the Supplementary Material. For the random packing a similar procedure was used, leading to maximal contact areas of 7.5% of the cross-sectional area of an individual particle. In this case, smaller contact areas were present as well, originating from particles that were not yet, but almost in contact before the procedure. In case of the sc packing (ε_e=0.40) shown in Fig. 1c, particles overlap automatically and no shrinkage was applied (contact surface is 10% of the particles' cross sectional area). Note that for this packing geometry the contact areas are located at the side walls of the cubic cell.

All packings studied contained uniformly sized particles with a diameter (d_p) of 2.00 µm and a core of 1.26 µm, corresponding a core to particle ratio ρ of 0.63. The resulting unit cell sizes are given in Fig. 1.

2.2. Computational mesh

The investigated geometries were meshed with Ansys® Meshing, version 17.1 from Ansys, Inc. In case of the ordered packings, the mesh cell sizes were chosen such that each eighth of a particle contained at least 225.000 tetrahedral cells. Cell sizing was similar in the fluid zones. At the interfaces (core/shell and shell/mobile zone) 3 thin layers of triangular prism cells (inflation layers) and a sizing function was used to ensure smaller cells near these regions as here the steepest temperature gradients were expected. The sizing of the mesh cells was such that quadrupling the number of cells had an impact of less than 0.1% on the measured effective conductivity coefficient. The random packing contained 3.2×10^6 tetrahedral cells, resulting in 2.4×10^3 cells per particle. Cells sizes were smallest near the interfaces.

As a grid check, the sc packing was meshed with the same settings as the random packing (also yielding 2.4×10^3 cells per particle) and used with some typical material conductivities, resulting in a maximal error on the effective conductivity of 1.2%. This is a good measure for the accuracy of the effective thermal conductivities determined for the random packing.

2.3. Boundary conditions

Velocity was zero throughout the entire domain. At velocities typically employed in HPLC separations, fluid motion has no influence on the effective conductivity [20]. The top and bottom were assigned a temperature of 400 K and 300 K respectively. A symmetry boundary condition ($\frac{dT}{dn} = 0$) was applied at the four other outer surfaces for the ordered packings, while a periodic boundary condition was applied to the side walls of the random packing.

2.4. Simulation procedure

The energy equation (which describes the conservation of energy principle) [21] was solved using the finite volume solvers of Ansys® Fluent, version 17.1 from Ansys, Inc. to find the steady-state temperature field (see Fig. 2 for example). Because of the steady-state and because fluid velocity was zero at any point the only relevant term left in the energy equation is the heat conduction term, yielding:

$$\frac{\partial}{\partial x}\left(\frac{\partial T}{\partial x}\right) + \frac{\partial}{\partial y}\left(\frac{\partial T}{\partial y}\right) + \frac{\partial}{\partial z}\left(\frac{\partial T}{\partial z}\right) = 0 \qquad \text{(2a)}$$

Or shorthand with ∇ · for divergence, ∇ for gradient and T the temperature field:

$$\nabla \cdot (k\nabla T) = 0 \tag{2b}$$

The least squares cell-based method was used for gradient evaluation.

2.5. Calculation of k_{eff}

Fourier's heat transfer law (Eq. 1) can be used to express the steady-state heat transfer (Q [W]) through an infinitely wide slab of finite thickness Δx and consisting of a homogeneous material with thermal conductivity k_{eff} [21]:

$$Q = -k_{eff} A \frac{\Delta \mathrm{T}}{\Delta x} \tag{3}$$

with ΔT the temperature difference between the top and bottom surface of the slab.

Taking the steady-state heat flux Q reported by the software, and using the known ΔT (=100 K) and Δx (see Fig. 1 for values), Eq. (3) readily allows to calculate k_{eff}.

2.6. Hardware

All simulations were performed on Dell Power Edge R210 RackServers each equipped with an Intel Xeon x3460 processor (clockspeed 2,8 GHz, 4 cores) and 16 Gb, 1333 MHz ram memory, running on Windows server edition 2008 R2 (64-bit). Simulations of the steady-state temperature field in the aforementioned geometries took about 100s for the random geometry (parallel on 3 cores), while the ordered packings took about 40s (on a single core).

2.7. Numerical validation

The effective medium theory provides a number of well-established and highly accurate solutions for the effective thermal conductivity k_{eff} in a composite medium [13,22-26]. For an fcc packing of fully porous spheres for example, k_{eff} can be very accurately calculated using [27]:

$$k_{eff} = k_m \left(1 - \frac{3(1-\varepsilon_e)}{\mathrm{D}}\right) \tag{4a}$$

$$\begin{aligned} \mathrm{D} = & -\beta_1^{-1} + (1-\varepsilon_e) + c_1\beta_3(1-\varepsilon_e)^{10/3} + c_2\beta_5(1-\varepsilon_e)^{14/3} \\ & + c_3\beta_3^2(1-\varepsilon_e)^{17/3} + c_4\beta_7(1-\varepsilon_e)^6 + c_5\beta_3\beta_5(1-\varepsilon_e)^7 \\ & + c_6\beta_9(1-\varepsilon_e)^{22/3} + O\left((1-\varepsilon_e)^{25/3}\right) \end{aligned} \tag{4b}$$

$$\beta_i = \frac{\alpha - 1}{\alpha + \frac{i+1}{i}} \qquad i = 1, 3, 5, \ldots \tag{4c}$$

$$\alpha = \frac{k_{pz}}{k_m} \tag{4d}$$

with k_{pz} the thermal conductivity of the porous zone. For a fully porous particle, the porous zone refers to the entire particle (while for a core-shell particle this refers only to the shell). The values of the constants c_1-c_6 can be found in [16].

Comparing our computed k_{eff}-values for non-contacting fcc sphere packings with the result derived from Eq. (4) shows our results have an accuracy on the order of 0.1%.

3. Results and discussion

3.1. Limits of thermal bed conductivity enhancement resulting from an increased core conductivity

In this part of the study, simulations were done using k_{pz}-values ranging between 0.36 W/(m·K) and 1.40 W/(m·K) to cover and exceed the typical range of possible heat conductivity values for a mesoporous silica layer filled with the typical mobile phases used in RPLC. The cited k_{pz}-values values were obtained by representing the shell layer as a packing of touching and even slightly overlapping nanospheres fully impregnated with mobile phase liquid (see SM). Fortunately, the degree of particle overlap and nanosphere arrangement only has a weak effect on the overall k_{pz}-value (see SM), such that all obtained values are in the same range. The k_{pz}-range considered for the simulations also comprises the values cited in [28].

Fig. 3a shows, for several typical values of the mobile and porous zone conductivity, how the effective bed conductivity can be expected to increase in an fcc packing with porosity 40% when the core conductivity would be raised from the current solid silica case (k_{core}≅1.40 W/(m·K)) to that of materials that are extremely good heat conductors such as gold (k=320 W/(m·K)) and copper (k=400 W/(m·K), out of scale on Fig. 3a). As can be noted, the increase in k_{eff} with respect to the case of a silica core is typically only of the order of some 40%. This is much less than assumed in [3] (where a 21-fold increase of the conductivity is anticipated). The strongly saturating trend of the curves also implies that any attempt to raise the core conductivity above that of alumina (k_{core}≅30 W/(m·K)) would be completely futile. Taking the derivative of the data in Fig. 3a (approximated through the first order forward difference) shows these decrease to zero, suggesting k_{eff} tends to an asymptotic value.

The height of the plateaus in Fig. 3a strongly depends on the thermal conductivity of the mobile phase. This effect is filtered out in Fig. 3b by making a dimensionless representation of the data shown in Fig. 3a, completed with a set of additional results for other k_{pz}/k_m-values. The data show that, for each given value of k_{pz}/k_m, there is always one unique curve describing how the relative bed conductivity k_{eff}/k_m varies with the relative ratio of k_{core}/k_m. The relative conductivity k_{eff}/k_m gives the increase in bed conductivity relative to the case of a tube without particles and only filled with mobile phase. This dimensionless representation has been added to show that an increase of the core conductivity beyond that of silica can never be expected to lead to more than a 25 to 50% increase in overall bed conductivity (for k_m=0.15 and 0.58 resp.).

Fig. 4 confirms the above observations (again showing an increase in k_{eff} with respect to the silica core case on the order of some 20-70% and asymptotic behavior at high k_{core}), but now for a broader range of packing geometries, including two ordered and one random sphere packing, all with contacting spheres. At this point, it should be noted that the ε_e=0.40 fcc-packing corresponds to a physically unrealistic case where the spheres are not in direct contact and are hanging without suspension in the medium. The same holds for the ε_e=0.40 bcc-packing. The ε_e=0.40 sc-case and the random packing case on the other hand correspond to cases where the spheres are in direct contact. As can be noted, the existence of a direct contact has some effect (maximally 7% at high k_{core} as can be derived from the difference between the ε_e=0.40 fcc-packing and the random packing case), but certainly not a huge one. The effect of the porosity itself is clearly much more important, as can be derived from the difference between the ε_e=0.40 fcc- and the ε_e=0.24 fcc-curves. Admittedly, this shift also includes a transition from a non-contacting to a contacting sphere case, but this effect is rather limited, as can be understood from the relatively small difference between the ε_e=0.24 fcc-curve and the ε_e=0.24 fcc (insulated)-curves, whereby the latter corresponds to a case where the contact zones between the spheres were insulated to eliminate the contribution of the contact effect. Given this relatively small difference, the main difference between the ε_e=0.40 fcc- and the ε_e=0.24 fcc-curves can be attributed to the fact that the latter corresponds to a case with significantly higher packing density and hence also with a higher density of (relatively strongly conducting) silica. The relatively strong ε_e-effect shows that, in order to properly investigate the effective conductivity of packed beds, it is more relevant to work at the proper external porosity than to correctly represent the contact mode of the spheres.

Despite the above, the literature reports [12,28-30] wherein core-shell particle columns have been shown to display a markedly larger effective conductivity than fully porous particle columns remain fully relevant. To investigate this with our numerical approach, Fig. 5 compares how k_{eff} varies with the porous zone conductivity k_{pz} in a fully-porous particle and a core-shell particle case. A first important observation from Fig. 5 is that the curves cross at some given k_{pz}-value. This crossing point originates from the fact that, when the porous zone becomes equally conductive as the core (k_{pz}=k_{core}), a core-shell particle will behave thermally as if it was a fully porous particle. It is then obvious to see that beds with the same packing arrangement and porosity consisting of either particle type have the same k_{eff}. In Fig. 5 the external porosities of both beds slightly differ causing the crossing point to shift (from k_{pz}=1.4 to 1.1 W/(m·K)). Another important observation from Fig. 5 is that the fully porous and core-shell particle case curves lie relatively close to each other in the range of k_{pz}-values pertaining to porous silica (greyed area).

The black upward arrows added to Fig. 5 indicate the k_{pz}-value assumed in a recent study [28] for respectively a typical fully porous (k_{pz}=0.40) and a typical core-shell particle (k_{pz}=0.60 W/(m·K)). Comparing the k_{eff}-values corresponding to these values (resp. k_{eff}=0.28 W/(m·K) and k_{eff}=0.42 W/(m·K), see upward arrows), it can be concluded that the difference in effective conductivity observed between fully porous and core-shell columns is not only caused by the effect of the core but also because of the predicted difference in conductivity of the porous zone material of which the particles are composed. Because of the differences in production process, the shell of core-shell particles is typically denser in silica than fully porous particles. Comparing the shift in k_{eff} one can expect solely from the presence of a core (upward arrow vs. downward arrow), it can be concluded the presence of the core can only be expected to lead to an increase from k_{eff}=0.28 W/(m·K) to k_{eff}=0.36 W/(m·K), considerably less than that expected based on the difference in k_{pz}.

3.2. Limitations of the Zarichnyak-model and improved modelling

The reason for the strong deviation between some literature reports [3,12,28-30] and the results of the present study (up to a 2000% increase expected in literature [3] vs. a 68% increase to be expected upon an increase of the core conductivity from silica to gold) is that these few available literature reports are mainly based on a simple model that was reported in a series of models by Zarichnyak and Novikov [31]. This particular model was originally developed for heterogeneous materials and assumes the material consists of two types of cubical zones, resp. with conductivity k_1 and k_2. The cubes are arranged in two layers. In each layer, the cubes are perfectly arranged in a rectangular grid. They obtained:

$$k_{eff} = k_1(\phi_1)^2 + k_2(\phi_2)^2 + 4\frac{k_1 k_2}{k_1 + k_2}\phi_1\phi_2 \tag{5}$$

with ϕ_1 and ϕ_2 being the respective volumetric fractions of cubes with conductivity k_1 and k_2.

Extensions of this model that take in account a third material and an infinite number of layers exist, but are not used in chromatography literature. In the latter, Eq. 5 is typically used in two or more consecutive steps to combine several materials with different thermal conductivities.

$$k_{eff} = k_m(\varepsilon_e)^2 + k_{part}(1-\varepsilon_e)^2 + 4\frac{k_m k_{part}}{k_m + k_{part}}(\varepsilon_e)(1-\varepsilon_e) \tag{6a}$$

$$k_{part} = k_{pz}(\phi_{shell})^2 + k_{core}(\phi_{core})^2 + 4\frac{k_{pz} k_{core}}{k_{pz} + k_{core}}\phi_{shell}\phi_{core} \tag{6b}$$

with: ϕ_{shell} = fraction of shell volume on particle volume

ϕ_{core} = fraction of core volume on particle volume

= 1- ϕ_{shell}

= ρ^3

ρ = the ratio of core diameter to particle diameter

As can be noted from the modelling lines (dashed lines) added to Fig. 3b and 4, the curve representing Eq. (6) fits nicely to the data in the region of the silica conductivity, but completely deviates from the numerically computed values in the range of larger conductivities where gold and copper are situated.

The failure of the Zarichnyak-model in case of highly conducting cores can be explained by the fact the model assumes only two layers of cubes resulting in a considerable fraction of two-cube piles consisting of only the high conducting material. These then form a continuous, high conducting path through the entire model. The occurrence of such a high conductivity path running across the entire bed obviously does not apply to a bed of particles with high conductivity cores, as these cores are insulated from their surroundings by the lower conductivity shell and the mobile phase in the interstitial particle space. Because of the simplicity of its underlying assumptions, the Zarichnyak-model doesn't discriminate between the different packing arrangements. Therefore, Fig. 4 only shows two Zarichnyak-based curves: one for the low porosity fcc packing and another for all four (fcc, bcc, sc and random) high porosity (ε_e=0.39-0.40) packings.

Given the large similarity between the conduction of heat and the diffusion of species, and building upon our previous work regarding the improved modelling of the effective longitudinal diffusion using the so-called effective medium theory [16-18], it seemed straightforward to investigate how well this general theoretical framework can be used to model the trends observed in Figs. 3-4. The effective medium theory is based upon the seminal work of James Clerk Maxwell on the prediction of the effective electrical conductivity in composite media with high and low conductivity zones, and has later been extended to cover a broader range of geometries and to other conduction modes in a vast body of literature [13,14,22-27]. In this work, we have adapted the effective medium theory expressions originally derived by Torquato [32] to account for the geometry of the presently considered ternary system consisting of a first discrete medium with conductivity k_1, surrounded by a shell consisting of a second medium with conductivity k_2, embedded in a continuous medium with conductivity k_3. The resulting expression is given by:

$$k_{eff} = \frac{1 + 2\beta_1(1-\varepsilon_e) - 2{\beta_1}^2\zeta_2\varepsilon_e}{1 - \beta_1(1-\varepsilon_e) - 2{\beta_1}^2\zeta_2\varepsilon_e} k_m \tag{7a}$$

with:

$$\beta_1 = \frac{{k_{part}}/{k_m} - 1}{{k_{part}}/{k_m} + 2} \tag{7b}$$

$$k_{part} = \frac{1 + 2\gamma_1(1-\phi_{shell})}{1 - \gamma_1(1-\phi_{shell})} k_{pz} \tag{8a}$$

$$\gamma_1 = \frac{{k_{core}}/{k_{pz}} - 1}{{k_{core}}/{k_{pz}} + 2} \tag{8b}$$

wherein ζ_2 is the three-point parameter. To arrive at Eq. (7), we started from a formula derived by Hashin and Shtrikman in [33] that gives the effective conductivity of a sphere consisting of a spherical core surrounded by a concentric shell (Eq. 8). The resulting average or effective thermal conductivity of the particle (k_{part}) is subsequently used in Torquato's expression (Eq. 7) to average this particle conductivity with the conductivity of the mobile phase (k_m) present in the interstitial space between the particles. Eq. (7) can be used for different types of particle arrangements by using the appropriate value for the three-point parameter (ζ_2). This value depends, evidently on the type of arrangements (fcc, bcc, random, …) and also on the external porosity. ζ_2-values for different packing arrangements can be found in [16,34].

As can be noted from the full line curves added to Figs. 3b and 4, Eq. (7) is much better suited than the Zarichnyak-model (Eq. 6) to represent the effective heat conductivity over the entire range of possible k_{core}-values. The remaining differences between the numerical data and the model curves based upon Eq. (7) are not due to simulation errors (cf. the 0.1% accuracy of the data shown in Section 2.2) but are a consequence of the limitations of the assumptions underlying Eq. (7). Although the theory is less well developed for cases where the high conductivity zones are in direct contact, the superiority of Eq. (7) over Eq. (6) is undisputed. The ζ_2-values used in Fig. 4 are given in the caption. These were taken from [32] for the ε_e=0.40 bcc and fcc packing and from [18] for the random packing. In case of the fcc packing with ε_e=0.24 and the sc packing (with ε_e=0.40), no values are available in literature at these porosities. Therefore, ζ_2 was determined by fitting Eq. 7 to the simulation data.

3.3. Other possibilities for thermal bed conductivity enhancement

Since the preceding results have made it clear that the use of highly conducting cores cannot be expected to lead to the predicted strong increase of the overall bed conductivity, we found it instructive to investigate which other alternatives would be better suited. The first alternative we explored was the use of highly conductive shells, as opposed to using highly conductive cores. As can be observed from Fig. 6, the use of highly conductive shells would indeed be much more effective than the use of highly conducting cores, if ever such highly conducting porous material could be made. The increase in k_{eff} that could be expected if the conductivity of the porous shell material could be freely increased would extend over at least two orders of magnitude, hence completely overshadowing the potential increase in conductivity that can be expected when using highly conductive cores (cf. the saturating trend in Figs. 3-4). Interestingly, the Zarichnyak-model does not fail here and is capable of representing the observed, almost linear increase. This makes sense because the two layer variant of the Zarichnyak-model implies a bicontinuous medium, meaning both phases are continuous. When this assumption is applied in a first step to the core and shell, the error is small because the cores are not continuous but anyhow contribute little compared to the high conducting shells. In the second step, the particles and mobile zone are both continuous (in agreement with the model assumption). In case of highly conducting cores (Figs. 3-4) the error introduced by using the Zarichnyak equation in the first step is much larger, as can be observed from Fig. 3b-4.

Returning to the case of highly conducting shells, it is now the Torquato-model given by Eq. (7) that completely fails (data not shown). This is due to the fact that the particles are in contact and hence form a continuous phase, while this model assumes one continuous (the mobile zone) and one discontinuous phase (the particles) in the second step. This leads to small errors for poorly conducting particles (Figs. 3-4), but to large errors for well conducting particles. To correct for this, an inverted Torquato-expression, in which the well-conducting particles are treated as the continuous phase and the poorly conducting mobile phase is treated as the discontinuous phase, can be derived:

$$k_{eff} = \frac{1 + 2\beta_1'(\varepsilon_e) - 2{\beta_1'}^2\zeta_1(1-\varepsilon_e)}{1 - \beta_1'(\varepsilon_e) - 2{\beta_1'}^2\zeta_1(1-\varepsilon_e)} k_{part} \tag{9a}$$

with:

$$\beta_1' = \frac{{k_m}/{k_p} - 1}{{k_m}/{k_p} + 2} \tag{9b}$$

wherein k_{pz} is calculated using Eq. (8a-b) and ζ_1 is the three-point parameter of the mobile zone and is equal to 1-ζ_1 according to [32].

As can be noted in Fig. 6, this curve is better suited to describe the almost linear increase of k_{eff} with k_{pz} for well conducting shells (high k_{pz}). Given the very strong dependency of the effective bed conductivity with the shell conductivity observed in Fig. 6, it is clear that any material with a higher conductivity than porous silica would have an immediate positive effect on the bed conductivity. A possible material choice for the shell would be diamond. This material combines a very high conductivity (k=900-2320 W/(m·K) [35]) with some other properties beneficial for chromatographic purposes. Diamond has a high chemical inertness, mechanical, thermal and hydrolytic stability and shows no shrinking or swelling in the presence of inorganic or organic solvents [36]. It exists in porous forms and its surface can be functionalized [36]. Furthermore, it can be synthetically produced for a lower cost than natural diamond [36]. The use of diamond as stationary phase in HPLC is demonstrated in several publications [36-40].

Another approach to increase the overall bed conductivity would be to find a way to connect the cores of the particles such that they no longer act as insulated "islands". As shown in Fig. 7, a system of particles with connected cores (see Fig. 1e for the geometry of the cylindrical connection "bridges" running between adjacent cores that were considered to make the calculation) would indeed lead to a situation where the overall bed conductivity would increase linearly with an increase of the core conductivity. Obviously, such a system is artificial, but it is the only conceivable way to benefit significantly from the possibility to use cores made from a highly conducting material such as alumina or cupper. This can be readily observed when comparing the "no core contact" data set that was added to Fig. 7 (same sc packing as used in Fig.4) with the two other cases where the cores are linked and for which the k_{eff}-values follow a continuously increasing trend with increasing k_{core}. Provided the contact area between the cores would be sufficiently high, this increase would follow a linear dependency (cf. the fact that the curves for the different contact area values become gradually more linear). Although the geometry considered here (sc-arranged core-shell particles with "bridges" running between the cores, see Fig. 1e) is far from realistic, the result suggests that any structure having a backbone of interconnected highly conducting material (such as for example a monolithic metal skeleton cladded with a meso-porous silica layer) would provide a good solution to radially remove the frictional heat from UHPLC columns.

4. Conclusions

The use of highly conducting cores made of materials such as alumina or gold can be expected to lead to much smaller increases of the overall bed heat conductivity than previously assumed based on an extrapolation of the Zarichnyak-model. The present, well-validated numerical study has shown this model severely overestimates the bed conductivity in the case of high conductivity cores because the model overestimates the probability to form continuous high conductivity paths through the bed. Other, much more accurate models can be derived from the Effective Medium Theory. These fit the computed data much more faithfully and provide an explanation for the strongly saturating trend in the relation between the overall bed heat conductivity (k_{eff}) and the conductivity of the core (k_{core}). This saturating trend can be attributed to the fact that the cores are completely surrounded by less conducting porous zone which acts as a thermal insulator in that case.

It was also found that the presence of a silica core has a smaller effect on the overall bed conductivity than previously assumed and that the differences in bed conductivity reported in literature between fully-porous and core-shell particles are, besides the presence of the core, also due to differences in the conductivity of the meso-porous material of which commercial fully-porous and core-shell particles are being composed.

Finally, it was also shown that the most efficient way to increase the bed conductivity would be to 'break' through the thermal insulation around the cores by bringing them in thermal contact through bridge-like connections or by using highly conducting materials for the shell layer. Both approaches are at present however still purely speculative, but future developments in fabrication technology (e.g. 3D printing) could change this situation.

Acknowledgements

Deridder S. gratefully acknowledges a research grant from the Research Foundation – Flanders (FWO-Vlaanderen).

References

[1] K. Broeckhoven, G. Desmet, Considerations for the use of ultra-high pressures in liquid chromatography for 2.1mm inner diameter columns, J. Chromatogr. A 1523 (2017) 183-192.
DOI: 10.1016/j.chroma.2017.07.040.

[2] G. Guiochon, The limits of the separation power of unidimensional column liquid chromatography, J. Chromatogr. A, 1126 (2006) 6-49.
DOI: 10.1016/j.chroma.2006.07.032.

[3] J. Kostka, F. Gritti, K. Kaczmarski, G. Guiochon, Modified Equilibrium-Dispersive Model for the interpretation of the efficiency of columns packed with core-shell particle, J. Chromatogr. A 1218 (2011) 5449-5455.
DOI: 10.1016/j.chroma.2011.06.019.

[4] K. Broeckhoven, J. Billen, M. Verstraeten, K. Choikhet, M. Ditmann, G. Rozing, G. Desmet, Towards a solution for viscous heating in ultra-high pressure liquid chromatography using intermediate cooling, J. Chromatogr. A 1217 (2010) 2022-2031.
DOI: 10.1016/j.chroma.2010.01.072.

[5] S.F.A. Talib, W.H. Azmi, I. Zakaria, W. Mohamed, A.M.I. Mamat, H. Ismail, W.R.W. Daud, Thermophysical Properties of Silicon Dioxide (SiO2) in Ethylene Glycol/Water Mixture for Proton Exchange Membrane Fuel Cell Cooling Application, Energy Procedia 79 (2015) 366-371. DOI: 10.1016/j.egypro.2015.11.504.

[6] R.H. Perry, D.W. Green, Perry's Chemical Engineers' Handbook, 7th ed., McGraw-Hill, New York, 1997.

[7] H. Poppe, J.C. Kraak, J.F.K. Huber, J.H.M. van den Berg, Temperature-gradients in HPLC Columns due to Viscous Heat Dissipation, chromatographia 14 (1981) 515-523. DOI: 10.1007/bf02265631.

[8] H. Poppe, J.C. Kraak, Influence of thermal conditions on the efficiency of high-performance liquid chromatographic colummns, J. Chromatogr. 282 (1983) 399-412. DOI: 10.1016/S0021-9673(00)91617-0.

[9] A. de Villiers, H. Lauer, R. Szucs, S. Goodall, P. Sandra, Influence of frictional heating on temperature gradients in ultra-high-pressure liquid chromatography on 2.1 mm I.D. columns, J. Chromatogr. 1113 (2006) 84-91. DOI: 10.1016/j.chroma.2006.01.120.

[10] I. Halász, R. Endele, J. Asshauer, Ultimate limits in High-Pressure Liquid Chromatography, J. Chromatogr. 112 (1975) 37-60. DOI: 10.1016/S0021-9673(00)99941-2.

[11] F. Gritti, M. Gilar, J. A. Jarrell, Quasi-adiabatic vacuum-based column housing for very high-pressure liquid chromatography, J. Chromatogr. A 1456 (2016) 226–234. DOI: 10.1016/j.chroma.2016.06.029

[12] J.P Grinias, D.S. Keil, J.W. Jorgenson, Observation of enhanced heat dissipation in columns packed with superficially porous particles, J. Chromatogr. A 1371 (2014) 261-264. DOI: 10.1016/j.chroma.2014.10.075

[13] S. Torquato, Random Heterogeneous Materials, Springer Science & BusinessMedia, New York, 2002.

[14] Z. Hashin, Analysis of Composite Materials - A Survey, J. Appl. Mech. 50 (1983) 481-505. DOI: 10.1115/1.3167081.

[15] M. Barrande, R. Bouchet, R. Denoyel, Tortuosity of porous particles, Anal. Chem. 79 (2007) 9115-9121. DOI: 10.1115/1.3167081

[16] G. Desmet, S. Deridder, Effective medium theory expressions for the effective diffusion in chromatographic beds filled with porous, non-porous and porous-shell particles and cylinders. Part I: Theory, J. Chromatogr. A 1218 (2011) 32-45.
DOI: 10.1016/j.chroma.2010.10.087.

[17] S. Deridder, G. Desmet, Effective medium theory expressions for the effective diffusion in chromatographic beds filled with porous, non-porous and porous-shell particles and cylinders. Part II: Numerical verification and quantitative effect of solid core on expected B-term band broadening, J. Chromatogr. A 1218 (2011) 46-56.
DOI: 10.1016/j.chroma.2010.10.086.

[18] S. Deridder, G. Desmet, Calculation of the geometrical three-point parameter constant appearing in the second order accurate effective medium theory expression for the B-term diffusion coefficient in fully porous and porous-shell random sphere packings, J. Chromatogr. A 1223 (2012) 35-40.
DOI: 10.1016/j.chroma.2011.12.004.

[19] F. Gritti, G. Guiochon, Theoretical investigation of diffusion along columns packed with fully and superficially porous particles, J. Chromatogr. A 1218 (2011) 3476-3488.
DOI: 10.1016/j.chroma.2011.03.063.

[20] F. Gritti, G. Guiochon, Complete temperature profiles in ultra-high-pressure liquid chromatography columns, Anal. Chem. 80 (2008) 5009-5020.
DOI: 10.1021/ac800280c

[21] Y.A. Çengel, Heat transfer: a practical approach, 2nd ed., McGraw-Hill, New York, 2003.

[22] L. Rayleigh, On the influence of obstacles arranged in rectangular order upon the properties of a medium, Philos. Mag. 34 (1892) 481-502.
DOI: 10.1080/14786449208620364

[23] J.C.M. Garnett, Colours in metal glasses and in metallic films, Philos. T. R. Soc. Lond. 203 (1904) 385-420.
DOI: 10.1098/rsta.1904.0024

[24] J.C.M. Garnett, Colours in metal glasses, in metallic films and in metallic solutions, Philos. T. R. Soc. Lond. 205 (1906) 237-288.
DOI: 10.1098/rsta.1906.0007

[25] R. Landauer, The Electrical Resistance of Binary Metallic Mixtures, J. Appl. Phys. 23 (1952) 779-784.
DOI: 10.1063/1.1702301

[26] D.A.G. Bruggeman, Berechnung verschiedener physikalischer Konstanten von heterogenen Substanzen. 1. Dielektrizitätskonstanten und Leitfahigkeiten der Mischkörper aus isotropen Substanzen Ann. Phys. 416 (1935) 636-664.
DOI: 10.1002/andp.19354160705

[27] H. Cheng, S. Torquato, Effective conductivity of periodic arrays of spheres with interfacial resistance, P. Roy. Soc. A-Math. Phy. 453 (1997) 145-161.
DOI: 10.1098/rspa.1997.0009

[28] F. Gritti, G. Guiochon, Mass transfer resistance in narrow-bore columns packed with 1.7 µm particles in very high pressure liquid chromatography, J. Chromatogr. A 1217 (2010) 5069-5083.
DOI: 10.1016/j.chroma.2010.05.059

[29] D.V. McCalley, Some practical comparisons of the efficiency and overloading behaviour of sub-2 µm porous and sub-3 µm shell particles in reversed-phase liquid chromatography, J. Chromatogr. A 1218 (2011) 2887-2897.
DOI: 10.1016/j.chroma.2011.02.068

[30] F. Gritti, G. Guiochon, Comparison of heat friction effects in narrow-bore columns packed with core-shell and totally porous particles, Chem. Eng. Sci. 65 (2010) 6310-6319.
DOI: 10.1016/j.ces.2010.09.019

[31] Y.P. Zarichnyak, V.V. Novikov, Effective conductivity of heterogeneous systems with disordered structure, J. Eng. Phys. Thermophys. 34 (1978) 435-441.
DOI: 10.1007/BF00860269

[32] S. Torquato, Effective electrical conductivity of two-phase disordered composite media, J. Appl. Phys. 58 (1985) 3790-3979.
DOI: 10.1063/1.335593

[33] Z. Hashin, S. Shtrikman, A Variational Approach to the Theory of the Effective Magnetic Permeability of Multiphase Materials, J. Appl. Phys. 33 (1962) 3125-3131.
DOI: 10.1063/1.1728579

[34] D. Hlushkou, H. Liasneuski, U. Tallarek, S. Torquato, Effective diffusion coefficients in random packings of polydisperse hard spheres from two-point and three-point correlation functions, J. Appl. Phys. 118 (2015) 124901–1-124901–10.
DOI: 10.1063/1.4931153

[35] P.N. Nesterenko, P.R. Haddad, Diamond-related materials as potential new media in separation science, Anal. Bioanal. Chem. 396 (2010) 205-211.
DOI: 10.1007/s00216-009-3219-5

[36] A.A. Peristyy, O.N. Fedyanina, B. Paull, P.N. Nesterenko, Diamond based adsorbents and their application in chromatography, J. Chromatogr. A 1357 (2014) 68-86.
DOI: 10.1016/j.chroma.2014.06.044

[37] C. Hung, L.A. Wiest, B. Singh, A. Diwan, M.J.C. Valentim, J.M. Christensen, R.C. Davis, A.J. Miles, D.S. Jensen, M.A. Vail, A.E. Dadson, M.R. Linford, Improved efficiency of reversed-phase carbon/nanodiamond/polymer core-shell particles for HPLC using carbonized poly(divinylbenzene) microspheres as the core materials, J. Sep. Sci. 36 (2013) 3821-3829
DOI: 10.1002/jssc.201300988

[38] G. Saini, D.S. Jensen, L.A. Wiest, M.A. Vail, A.E. Dadson, M.L. Lee, V. Shutthanandan, M.R. Linford, Core-Shell Diamond as a Support for Solid-Phase Extraction and High-Performance Liquid Chromatography, Anal. Chem. 82 (2010) 4448-4456.
DOI: 10.1021/ac1002068

[39] D.A. Piper, J.A. Kareh, Chromatographic And Electrophoretic Separation Media And Apparatus, U.S. Patent Publication Number 20100278695, filed May 6, 2008.

[40] K.D. Wyndham, N.L. Wyndham, Composite Materials Containing Nanoparticles and their use in Chromatography, U.S. Patent 9,248,383, issued February 2, 2016.

Figure captions

Figure 1. Computational unit cells of the different considered packing geometries. Core material: dark grey, porous zone: grey, mobile phase: transparent blue. Red arrow indicates direction of heat flux from inlet to outlet plane (for all cells).

Figure 2. Example of a 3D steady state temperature profile computed in an fcc packing. Contours of the particles and cores shown in white. Conditions: k_{core}=1.4 W/(m·K), k_{pz}=1.4 W/(m·K), k_m=0.58 W/(m·K). Red=400 K, blue=300 K. Packing density: ε_e=0.40. Red arrow indicates direction of heat flux from inlet to outlet plane.

Figure 3a. Effect of the core conductivity (k_{core}) on the effective conductivity (k_{eff}) of an fcc core-shell packing for different porous zone and mobile phase conductivities (shown in figure). Packing parameters: ε_e=0.40, ρ=0.63. Model curves: Torquato-model, Eq. (7) with ζ_2=0.06 (Black lines).

Figure 3b: Dimensionless representation of the effect of the relative core conductivity (k_{core}/k_m) on the relative effective conductivity of the packing (k_{eff}/k_m) for different porous zone conductivities. Conditions: fcc packing ε_e=0.40, ρ=0.63, mobile phase conductivity: Black dots (●) =0.15 W/(m·K); triangles (△) =0.58 W/(m·K); squares (◇) =0.21 W/(m·K). Silica range given by grey box. Model curves: Torquato-model, Eq. (7) with ζ_2=0.06 (Black lines). Zarichnyak-model, Eq. (6) (Grey dotted lines).

Figure 4. Effect of the packing geometry on the relative effective conductivity (k_{eff}/k_m) for the case of k_{pz}/k_m=2.41. Simulation data: fcc packing (○), fcc packing with insulated contacts (Δ), sc packing (♦), fcc packing (✱), random packing (▲) and bcc packing (●). Model curves: Zarichnyak-model, Eq. (6) (dashed grey lines), Torquato-model, Eq. (7) with ζ_2=0.16 (FCC ε_e=0.24), 0.22 (SC), 0.06 (FCC ε_e=0.40), 0.27 (Random) and 0.08 (BCC) (full black lines).

Figure 5. Variation of the effective conductivity (k_{eff}) with the porous zone conductivity (k_{pz}) for the case of a random packing of fully porous (full line) and a core-shell particles (dashed line), according to the Torquato-model with ζ_2=0.18 (as in [34]) and ε_e=0.38 and 0.41 for the fully porous particle and core-shell particle packing respectively (as in [28]). Mobile phase conductivity k_m=0.20 W/(m·K) and k_{core}=1.4 W/(m·K) as in [28]. The grey box represents possible values for k_{pz} given silica shells filled with mobile phases of various thermal conductivities. Meaning of arrows is discussed in the text.

Figure 6. Effect of the relative shell conductivity (k_{pz}/k_m) on the relative effective conductivity (k_{eff}/k_m). Packing parameters and conditions: fcc ε_e=0.24; k_m=0.58 k_{core}=1.4. Model curves: Zarichnyak-model, Eq. (6) (grey, dotted line), inverse Torquato-model, Eq. (9) with ζ_2=0.84 (black, dashed line).

Figure 7. Relative effective bed conductivity (k_{eff}/k_m) in an artificial system of particles with cylindrical thermal bridges connecting the cores of core-shell particles packed in an SC configuration. Different contacting areas are considered (values of r_b shown in figure), and

compared to the same packing without connected cores (base case).Black lines are no model lines and solely added for visual support.

Figure 1:

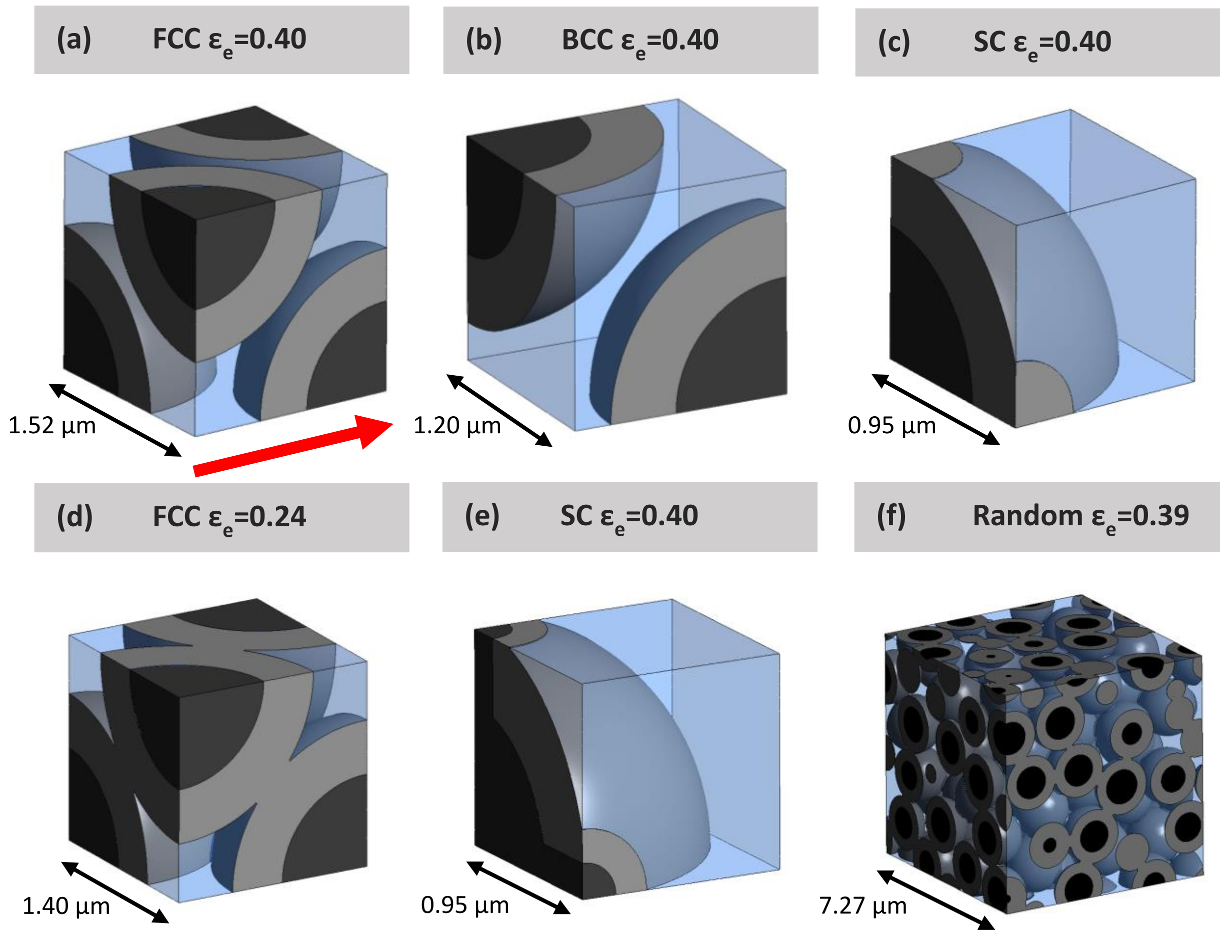

(a) FCC ε_e=0.40
(b) BCC ε_e=0.40
(c) SC ε_e=0.40
1.52 µm
1.20 µm
0.95 µm
(d) FCC ε_e=0.24
(e) SC ε_e=0.40
(f) Random ε_e=0.39
1.40 µm
0.95 µm
7.27 µm

Figure 2:

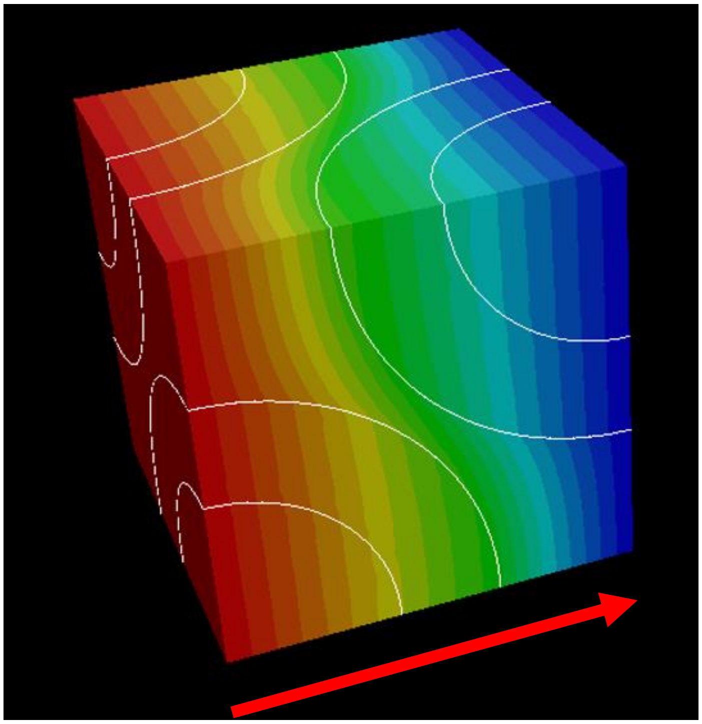

Fugure 3a:

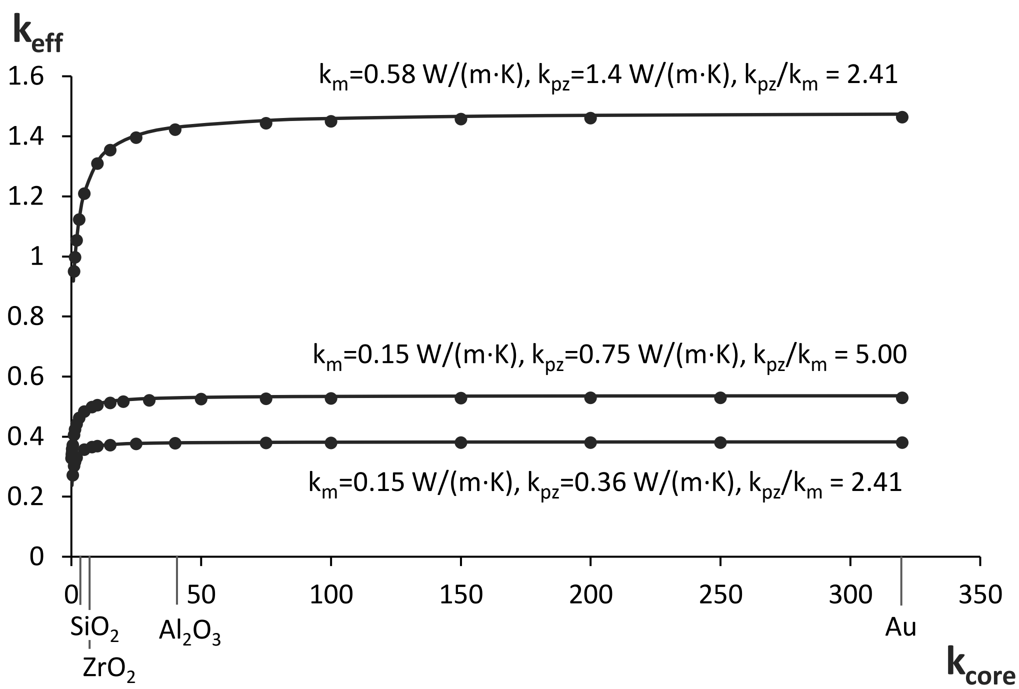

k_{eff}
1.6
1.4
1.2
1
0.8
0.6
0.4
0.2
0
k_m=0.58 W/(m·K), k_{pz}=1.4 W/(m·K), k_{pz}/k_m = 2.41
k_m=0.15 W/(m·K), k_{pz}=0.75 W/(m·K), k_{pz}/k_m = 5.00
k_m=0.15 W/(m·K), k_{pz}=0.36 W/(m·K), k_{pz}/k_m = 2.41
0
50
100
150
200
250
300
350
SiO_2
ZrO_2
Al_2O_3
Au
k_{core}

Figure 3b:

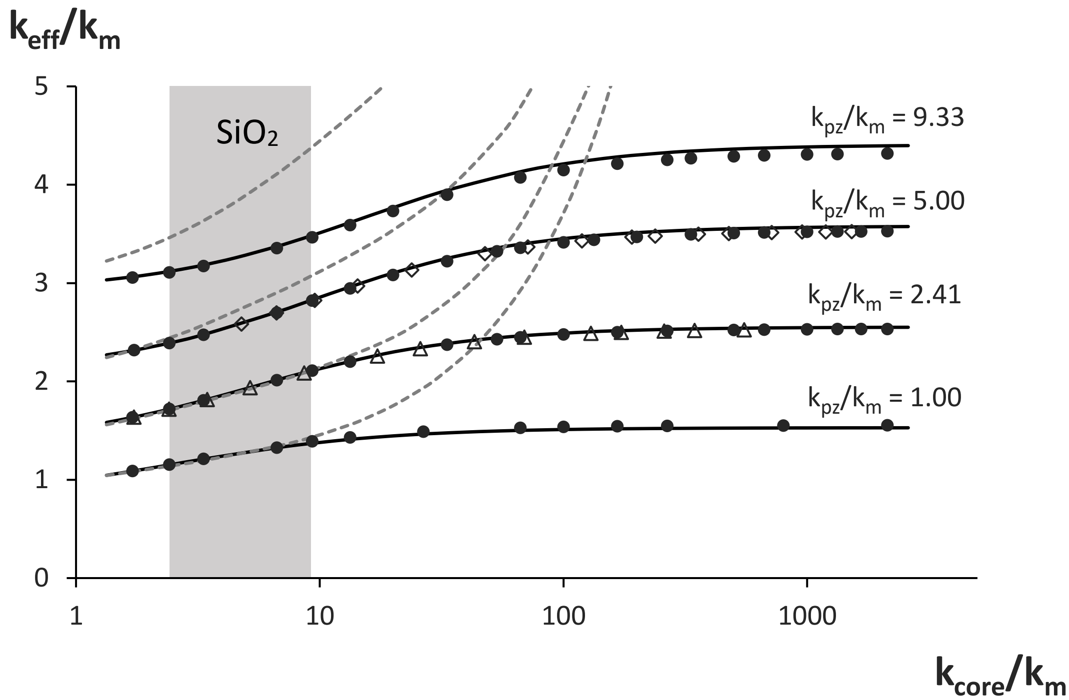

k_{eff}/k_m
5
4
3
2
1
0
SiO2
k_{pz}/k_m = 9.33
k_{pz}/k_m = 5.00
k_{pz}/k_m = 2.41
k_{pz}/k_m = 1.00
1
10
100
1000
k_{core}/k_m

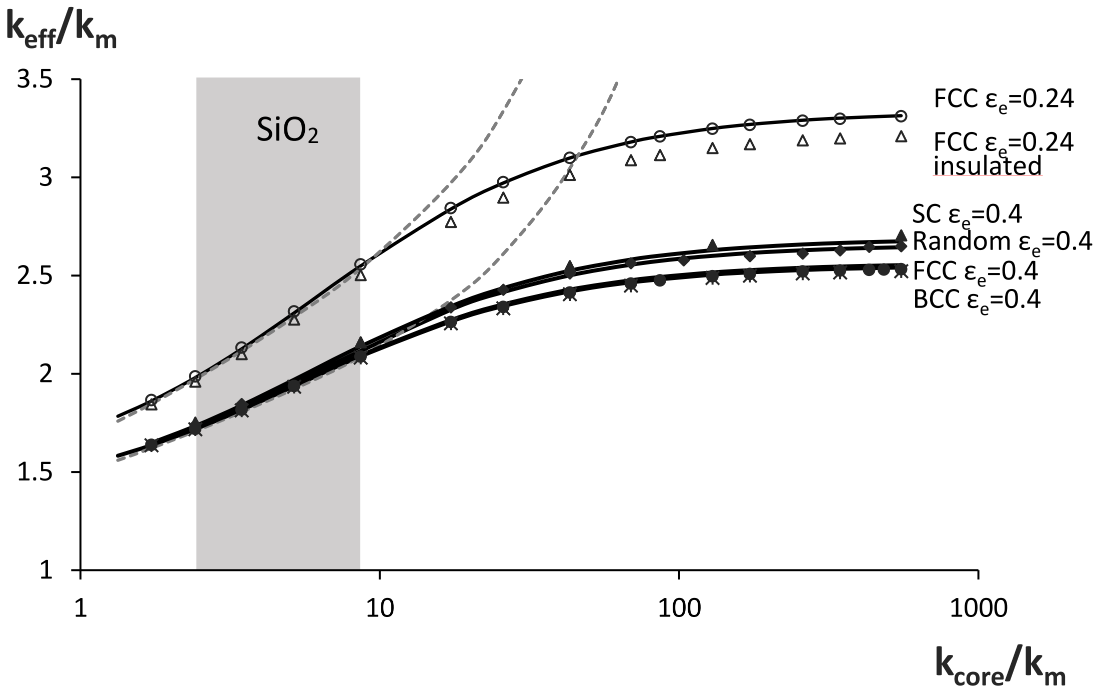

keff/km
3.5
3
2.5
2
1.5
1
1
10
100
1000
kcore/km
SiO2
FCC εe=0.24
FCC εe=0.24 insulated
SC εe=0.4
Random εe=0.4
FCC εe=0.4
BCC εe=0.4

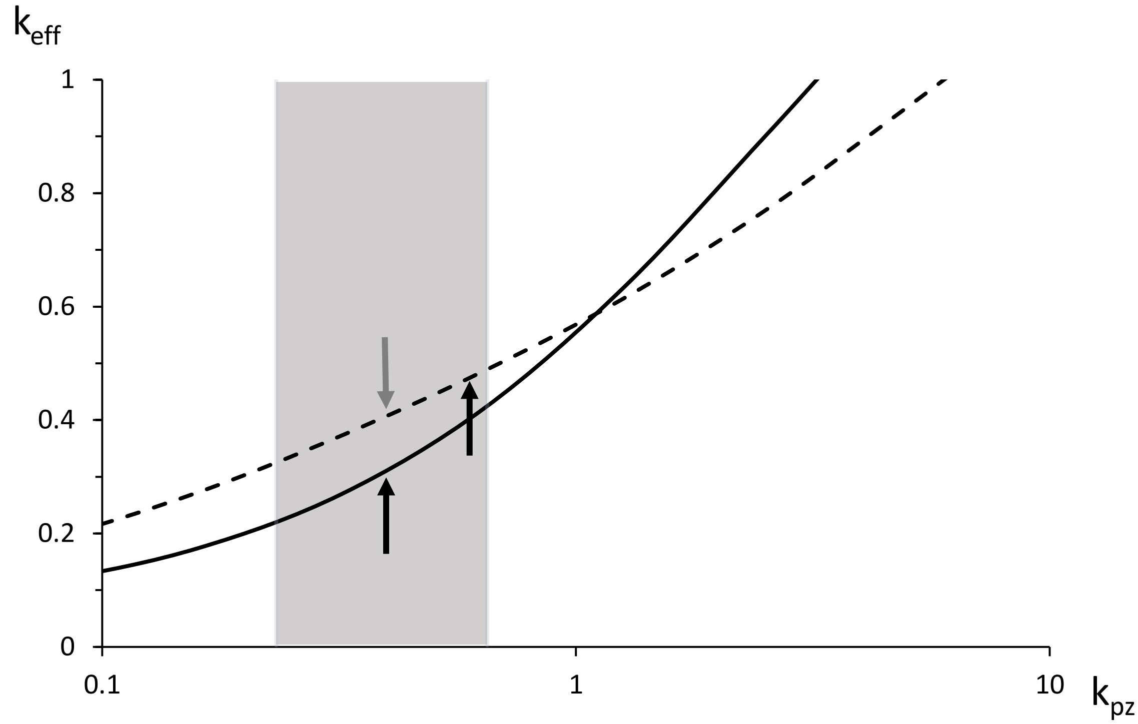

k_{eff}
1
0.8
0.6
0.4
0.2
0
0.1
1
10
k_{pz}

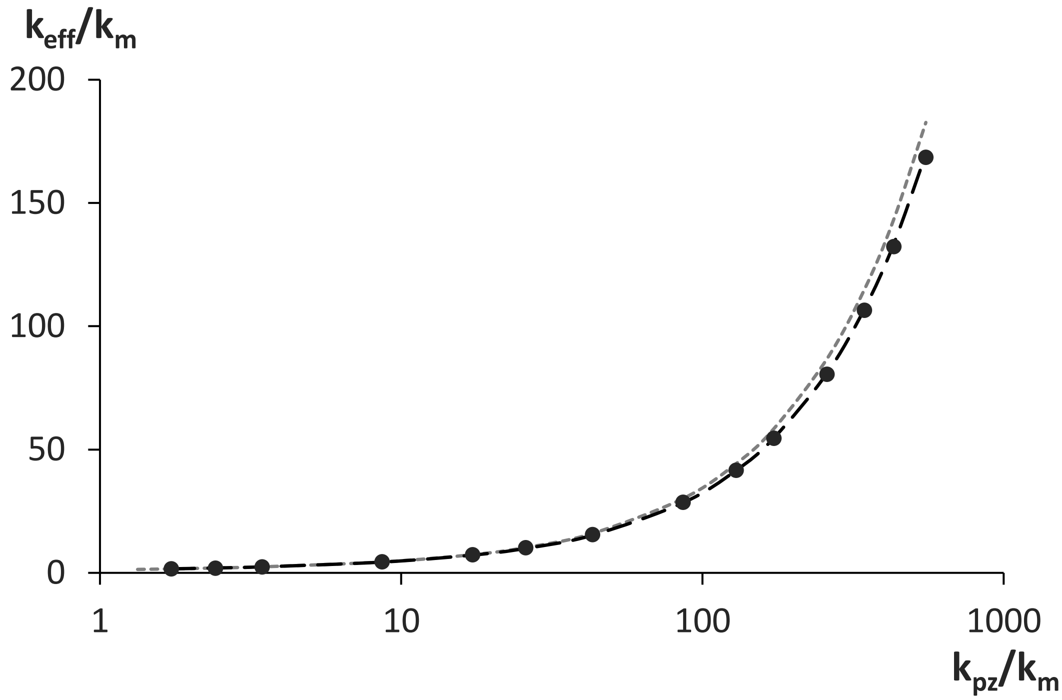

keff/km
200
150
100
50
0
1
10
100
1000
kpz/km

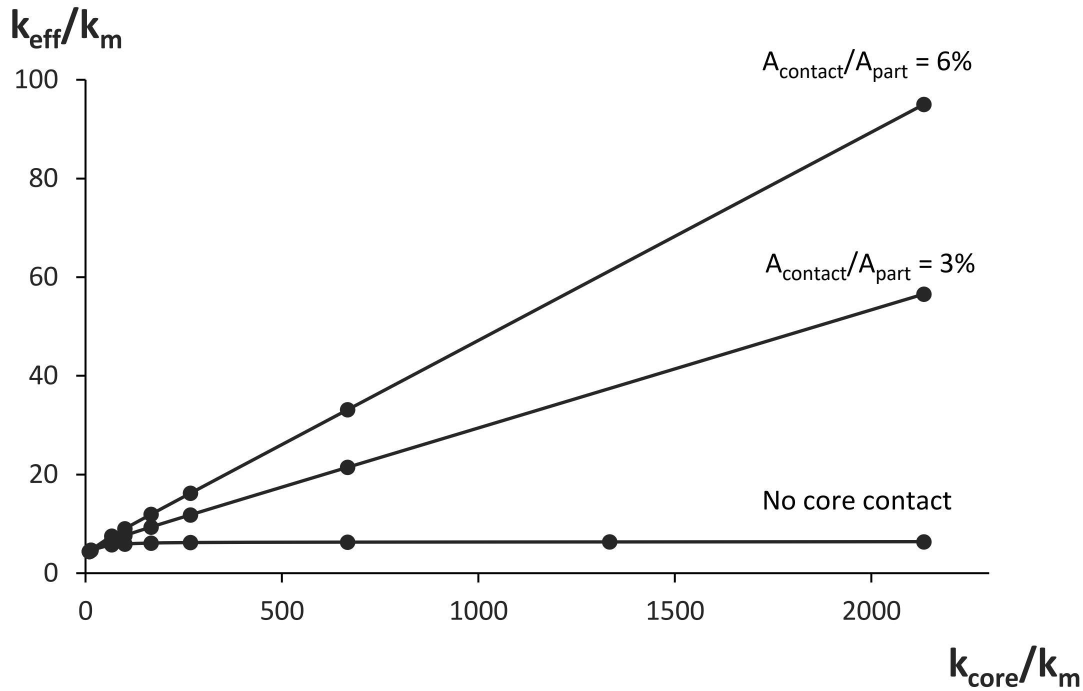

k_eff/k_m
100
80
60
40
20
0
0
500
1000
1500
2000
k_core/k_m
A_contact/A_part = 6%
A_contact/A_part = 3%
No core contact

Supplementary material:

Particle contact

To avoid numerical problems with singular contact points in the closest fcc packing case in Fig. 1d, the distance between neighboring particles was shrunk by 1%, thus creating a slight overlap. For meshing purposes, the sharp edge at the intersection of 2 neighboring particles was slightly chamfered, resulting in a "collar" of 1.0×10^{-8} m height between the particles (see Fig. SM1). The resulting contacting area between the spheres was always 3% of the cross sectional area of an individual particle. For the random packing a similar procedure (same shrinkage but larger chamfering, collar height 4.0×10^{-8} m) was used, leading to maximal contact areas of 7.5% of the cross-sectional area of an individual particle. In this case, smaller contact areas were present as well, originating from particles that were not yet, but almost in contact before the procedure. The chamfering procedure was also used for the sc packing in Fig. 1c. Given the specific packing geometry, this leads to a bigger contact surface (10% of the particles' cross sectional area).

Calculation of porous zone conductivity

While information on the average thermal conductivity of a particle bed is very scarce in chromatography literature, reports on the thermal conductivity of the particles themselves is non-existent to our knowledge, except for an estimation with the Zarichnyak-model in [28] which is questioned in the present publication. Therefore the thermal conductivity of the porous zone k_{pz} (from which k_{part} can be calculated with Eq. 8) was estimated through simulations. The porous zone was considered to consist of a packing of silica nanospheres. These were arranged in bcc and fcc packing and were slightly overlapping. The degree of overlap is characterized by the cross section of the overlap (A_i) divided by the cross section of the particle ($A_c=\pi.d_p^2/4$). In fig. SM2 it can be seen that the nanosphere arrangement and the amount of overlap have little effect on the porous zone conductivity. Because of the uncertainty on k_{pz}, the range of k_{pz}-values used in this study (0.36-1.40 W/(m·K)) comprises all possible values found in our simulations and the values reported in [28].

Figure SM1. (a) Two particles contacting in a single point. **(b)** Overlap due the shrinkage of the distance between the particle centers. For visualization purposes the shrinkage shown is 5 times bigger (5%) than that employed in the simulations (1%) **(c)** Sharp edge due to overlap **(d)** Collar due to chamfering. For visualization purposes a more profound chamfering was employed, resulting in a 5 times bigger collar height (0.05 µm) than that employed in the simulations (0.01 µm).

Figure SM2. Thermal conductivity of the porous zone (k_{pz}) as a function of the nanosphere overlap, for different values of k_m (as indicated on the figure). Nanospheres making up the porous zone are packed in an fcc arrangement **(a)** and bcc arrangement **(b)**.

Figure SM1:

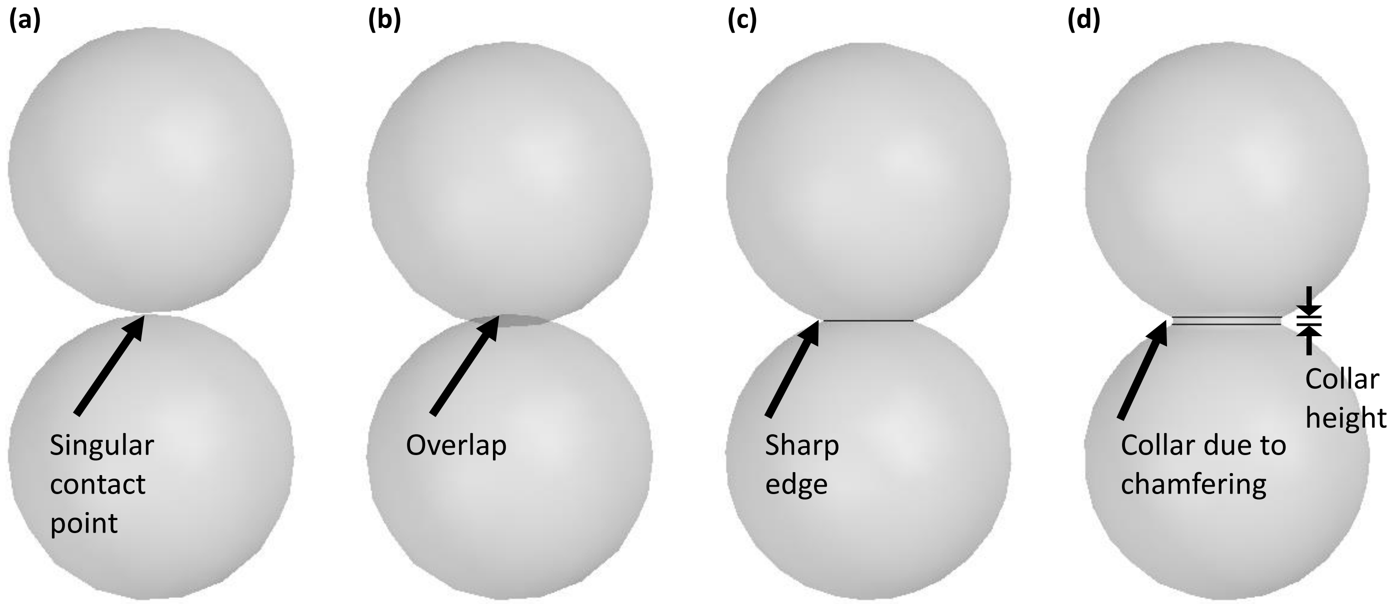
(a)
(b)
(c)
(d)
Singular contact point
Overlap
Sharp edge
Collar due to chamfering
Collar height

Figure SM2a

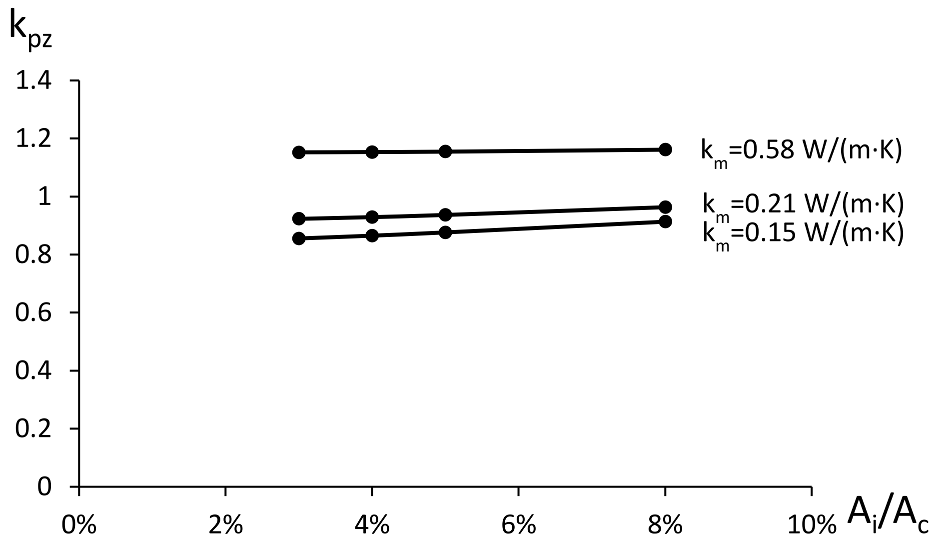

k_{pz}
1.4
1.2
1
0.8
0.6
0.4
0.2
0
0%
2%
4%
6%
8%
10%
A_i/A_c
k_m=0.58 W/(m·K)
k_m=0.21 W/(m·K)
k_m=0.15 W/(m·K)

Figure SM2b:

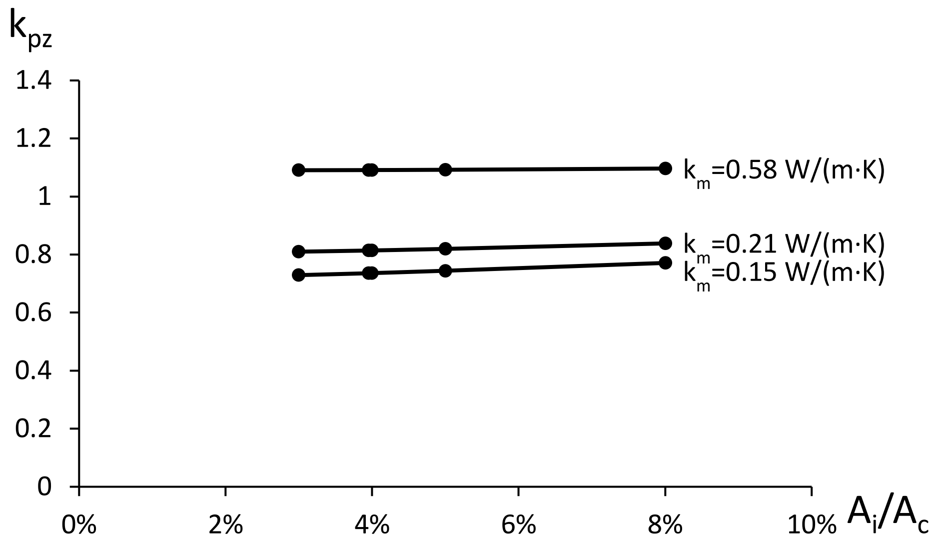

k_pz
1.4
1.2
1
0.8
0.6
0.4
0.2
0
0%
2%
4%
6%
8%
10%
A_i/A_c
k_m=0.58 W/(m·K)
k_m=0.21 W/(m·K)
k_m=0.15 W/(m·K)